

Identification of Novel 4-Oxo-4H-chromen-Hydroxamic Acid Derivative Targeting Selected HDAC Isoforms

Rosaline Ashraf, Mai Adel, Rabah A.T. Serya, Khaled A.M. Abouzid*

Department of Pharmaceutical Chemistry, Faculty of Pharmacy, Ain-Shams University, Cairo 11566, Egypt

ABSTRACT

Histone deacetylase inhibitors (HDACIs) represent a well-known class of compounds that exhibit potential therapeutic efficacy in a variety of diseases, particularly cancer and neurodegenerative disorders. This article discusses the development of compound **6** as a new HDAC inhibitor. It was designed based on the structure-activity relationship (SAR) of the previously reported HDAC inhibitors and the molecular modeling studies. Compound **6** was synthesized, and its structure was verified using different spectroscopic methods. It was biologically evaluated to assess its inhibitory activity against different HDAC isoforms, including HDAC1, 6, and 8. The results showed moderate inhibition against HDAC 1 and HDAC 8 over HDAC 6. It was also evaluated for its antineoplastic activity against the NCI 60 cancer cell line panel. The results revealed inhibitory activity against both the UO-31 renal cancer cell line and the BT-549 breast cancer cell line. Moreover, the Molecular modeling studies revealed a favorable binding affinity for the HDAC8 active site. These results suggest that compound **6** can be considered a promising candidate for the development of new selective class I HDACIs in the future.

Keywords: HDAC; Design; Synthesis; Molecular Modeling; Hydroxamic acid; Benzopyranone.

*Correspondence | Khaled A.M. Abouzid; Department of Pharmaceutical Chemistry, Faculty of Pharmacy, Ain-Shams University, Cairo 11566, Egypt. Email: Khaled.abouzid@pharma.asu.edu.eg

Citation | Ashraf R, Adel M, Serya RAT, Abouzid KAM, 2023. Identification of Novel 4-Oxo-4H-chromen-Hydroxamic Acid Derivative Targeting Selected HDAC Isoforms. Arch Pharm Sci ASU 7(2): 286-302

DOI: 10.21608/aps.2023.226661.1128

Print ISSN: 2356-8380. Online ISSN: 2356-8399.

Received 03 August 2023. Accepted 04 September 2023.

Copyright: ©2023 Ashraf *et al.* This is an open-access article licensed under a Creative Commons Attribution 4.0 International License (CC BY 4.0), which permits unrestricted use, distribution, and reproduction in any medium, provided the original author(s) and source are credited.

Published by: Ain Shams University, Faculty of Pharmacy

1. Introduction

Normally cells are divided according to a cell cycle that is monitored by many genes which are responsible for the growth rate, division, life span, and arresting the abnormal cells subsequently, this requires a balance between gene expression and silencing [1]. DNA and histones collaborate in regulating the process of gene transcription. DNA typically clumps together with histone proteins before being inserted into the nucleus as chromatins [2]. The degree of DNA enfolding around the histones is one of the major driving forces for gene expression and this is controlled by two families of enzymes called HATs (histone acetylases) and

HDACs (histone deacetylases). Histones have terminal lysine residues. The acetylation of their amino groups by HATs hides the positive charges and hence reduces the attraction between DNA and histones allowing the unfolding of deoxyribonucleic acid and creating access for the transcription factors to bind to the template for granting the expression [3]. On the other hand, their deacetylation by HDACs reveals the positive charges of protonated amino residues which successively permit the attraction between the positively charged lysine residues of histones and the negatively charged phosphate groups of DNA enabling the wrapping of DNA around histones resulting in gene silencing [4].

Cancer is caused by accumulated genetic mutations that result in activating oncogenes which encode the abnormal division rates and differentiation. Also, these mutations inhibit the tumor suppressor proteins and apoptotic genes like p53 which are considered guardian proteins that detect mutations and induce apoptosis [5, 6]. The silencing of these guardians is associated with the overexpression of HDACs. This demonstrates the significant importance of HDACs in regulating cell growth, proliferation, and controlling gene expression. Elevated levels of HDACs are usually a sign of poor prognosis in cancer patients. Based on that, epigenetic treatments have been developed, particularly with the elevated resistance of cancer cells towards traditional chemotherapeutics and the unbearable side effects that evolved as a consequence of the non-selectivity of conventional agents [7]. The most popular Epigenetic therapeutic agents include DNMT inhibitors and HDAC inhibitors [8].

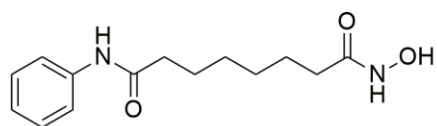
This study focuses on HDAC inhibitors which represent a promising class of epigenetic treatments, not only for cancer, but also for some cardiovascular diseases, neurodegenerative disorders, and inflammatory diseases [9]. HDACs family consists of 18 isoforms that can be categorized into two major categories based on their enzymatic activity. The first group involves the isoforms that rely on zinc for their catalytic activity. This group is further subdivided into 3 classes, namely, classes I, II, and IV that differ in their homology and distribution pattern [10]. Class I involves HDAC 1, 2, 3, and 8 which are localized in the nucleus and distributed in several tissues [11]. Class II is dissected into two subgroups, namely, classes IIa and IIb. Class IIa consists of HDACs 4, 5, 7, and 9 which are found in the nucleus and cytoplasm and control cellular differentiation. Class IIb comprises HDAC 6 and 10 isoforms that are situated in the cytoplasm and

affect mitosis [12, 13]. Class IV includes HDAC 11 with its distinctive structure [14]. The second main group of HDACs is NAD^+ dependent and consists of class III which covers the unique sirtuin deacetylases (SIRT 1-7) [15]. The use of HDAC inhibitors in cancer triggers the transcription of some suppressor proteins such as p53, which is responsible for apoptosis induction, and p21 which in turn inhibits the complexation between cyclin D and the protein kinase CDK4, prompting cell cycle arrest [16]. Furthermore, the inhibition of HDACs retards the progression of cancer cells by impeding their proliferation through modulating the level of Nanog expression which is the main transcriptional factor for the sustenance of cancer stem cells [17].

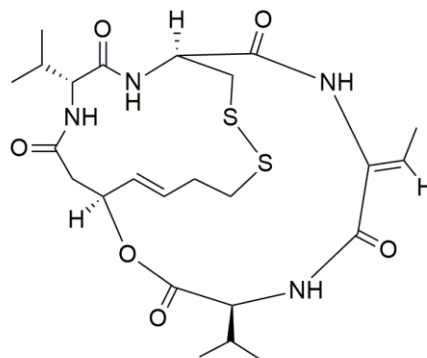
In the 1990s, the NCI discovered the first HDACI, trichostatin A (TSA), which is a naturally occurring small molecule hydroxamate. This encouraged scientists to develop synthetic HDACIs [18]. In 2006, the FDA approved the first hydroxamate-based HDACI developed by Merck which is Suberoylanilide Hydroxamic acid (SAHA) or Vorinostat which was released in the market with the trade name Zolinza[®] as a medication for cutaneous T-cell lymphoma (CTCL). The second FDA-approved HDACI is Romidepsin (Nusinersen) which is a benzamide-based compound that was developed by Celgene Pharmaceuticals and was placed on the market in 2009 under the trade name Istodax[®] for the treatment of multiple myeloma. In 2014, the third hydroxamate-based agent, Panobinostat was approved by FDA and marketed under the name of Farydak[®] for relapsed multiple myelomas. The last HDACI approved by FDA was in 2017 which is the benzamide-based Belinostat as a therapy for peripheral T-cell lymphoma (PTCL) and has the trade name of Beleodag[®] [19, 20]. Also, there are another two compounds that showed promising results and are under clinical

trials. These compounds are the benzamide derivative Chidamide and hydroxamate

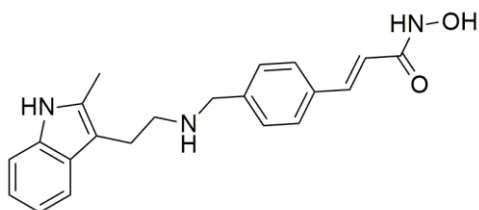
Pracinostat [21] (Fig. 1).



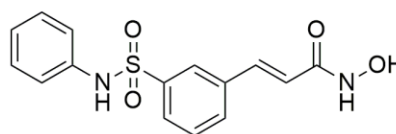
Vorinostat (SAHA)
Zolinza®
HDAC-1 IC₅₀ = 10 nM



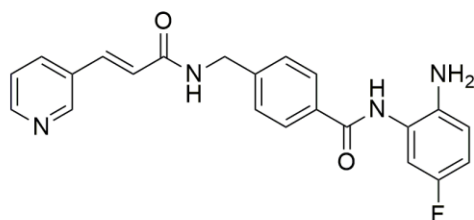
Romidepsin (Nusinersen)
Istodax®
HDAC-1 IC₅₀ = 36 nM



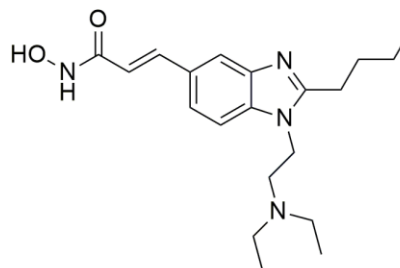
Panobinostat
Farydak®
HDAC-1 IC₅₀ = 1.4 nM
HDAC-8 IC₅₀ = 248 nM



Belinostat
Beleodag®
HDAC-1 IC₅₀ = 27 nM



Chidamide
HDAC-1 IC₅₀ = 95 nM
HDAC-8 IC₅₀ = 733 nM



pracinostat
HDAC-1 IC₅₀ = 49 nM
HDAC-8 IC₅₀ = 140 nM

Fig. 1. HDAC inhibitors authorized by the FDA

By extensive investigation of the reported HDAC inhibitors, it was observed that all share the same pharmacophoric features. The common pharmacophore can be divided into three parts as illustrated in Fig. 2. (1) **The capping group (SRM)**: interacts with the residues on the surface of the protein leading to the recognition and binding of the compound to the target. It is also defined in the literature by **surface recognition moiety (SRM)**. (2) **The linker**: it is responsible for the interactions in the narrow channel of the enzyme. The popular linkers vary between aliphatic, aromatic, and vinyl aromatic chains. (3) **The zinc-binding group (ZBG)**: is the most crucial

part of the activity. It is usually a bidentate chelating group [22, 23]. There are several ZBGs reported in literature usually classified into hydroxamates and non-hydroxamates. The hydroxamate refers to hydroxamic acid which is the most potent zinc chelating group and this is justified by its existence in TSA and three of the FDA-approved HDAC inhibitors (SAHA, Panobinostat, and Belinostat) that showed effective responses in nanomolar doses. The non-hydroxamates include any other metal chelating group, such as carboxylic acids, benzamides, thiols, mercaptoamides, sulfones, phosphenes, and trifluoromethyloxadiazolyl (TFMO) [24].

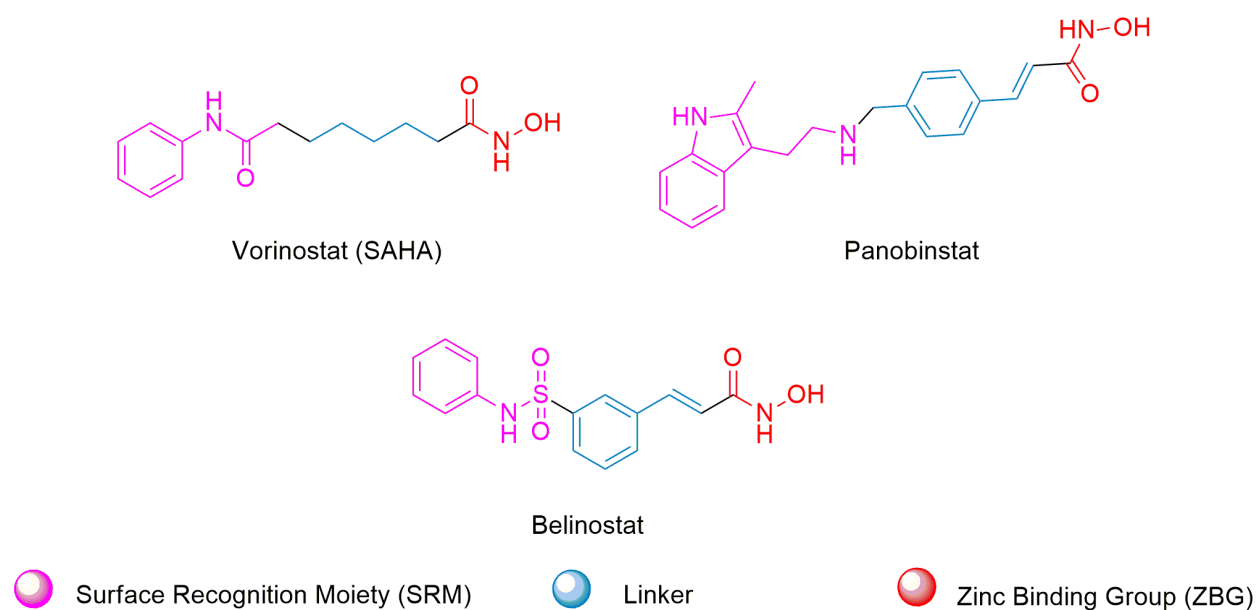


Fig. 2. The common pharmacophoric features of HDACIs

In this work, we are interested in designing a potent hydroxamate-based HDAC inhibitor. Also, we reported the synthesis, the spectroscopic analysis of the designed compounds, and the percent inhibition assay against HDAC 1, 6, and 8 isoforms at two different concentrations 1 and 10 μM . In addition, the synthesized compound was tested against the NCI cell lines panel at a single dose to detect its percent inhibition of the

growth of different cancer cells.

2. Material and Methods

2.1. Chemistry

2.1.1. Materials and Instrumentation

The starting materials and reagents utilized in this study were procured from renowned suppliers such as Sigma-Aldrich, Alfa-Aesar, or Apollo Scientific. The progression of reactions

was followed up by using Thin-layer chromatography (TLC), procured from Merck, and utilized UV light at a wavelength of 254 nm for visualization. Silica gel (230-400 mesh) was obtained from Sigma-Aldrich for performing column chromatography. Stuart Scientific apparatus was utilized for measuring the melting points without correction. Bruker 400 MHz spectrophotometer at the Center for Drug Discovery Research and Development, Ain Shams University, was used for recording Nuclear Magnetic Resonance (NMR) spectra where tetramethylsilane (TMS) served as a reference and dimethyl sulphoxide (DMSO) as a solvent. FT-IR spectra were obtained using a Thermo Scientific Nicolet iS10 spectrometer at the Drug Discovery Research and Development, Ain Shams University. High-Resolution Mass Spectrometry (HRMS) was conducted at the Natural Products Research Center, Fayoum University.

2.1.2. Experimental

2.1.2.1. 4-oxo-4H-chromene-3-carbaldehyde (1)

Yield 70% as white crystals, m.p. 158-160°C (as reported) [25].

2.1.2.2. (E)-3-(4-oxo-4H-chromen-3-yl)acrylic acid (2)

Yield 82% as pale yellow crystals [26], m.p. 253-254°C (as reported) [27].

2.1.2.3. (E)-ethyl4-(((4-oxo-4H-chromen-3-yl)methylene)amino)benzoate (3)

In a dry B19 flask, compound **1** (2 g, 11.5 mmol) and benzocaine (1.95 g, 11.5 mmol) were refluxed in 20 ml ethanol and a catalytic amount of glacial acetic acid for 12 hrs. Then the solution was cooled to RT. The resulting solid was collected by filtration and washed with ethanol. Then it was purified by column chromatography using hexane/ ethylacetate (6:1) as an eluting system then the product was recrystallized from

ethanol to yield the desired compound **3** as bright yellow crystals (0.2 g, 11%) m.p. 132-135°C. ¹H NMR (400 MHz, DMSO): δ 11.83 (d, 1H, CH=N), 8.20 (d, J = 12.2 Hz, 1H, ArH), 7.96 (d, J = 8.1, 2H, ArH), 7.85 (t, J = 7.7 Hz, 1H, ArH), 7.56-7.45 (m, 2H, ArH), 7.20 –7.07 (m, 2H, ArH), 5.86 (s, 1H, ArH), 4.30 (q, J = 7.3 Hz, 2H, CH₂-CH₃), 1.32 (t, J = 7.0 Hz, 3H, CH₂-CH₃). ¹³C NMR (101 MHz, DMSO): δ 181.02, 165.64, 156.06, 144.60, 144.26, 135.29, 131.42, 131.30, 126.17, 125.19, 122.79, 122.55, 121.67, 118.61, 116.71, 105.31, 101.55, 55.40, 14.68. FT-IR (ν max, cm⁻¹): 3066 (C-H aromatic), 2976 (C-H aliphatic), 1687 (C=O ester), 1644 (C=N), 1601 (C=C), 1463 (C-H bending aliphatic), 1264 (C-O). HRMS (ESI) m/z [M +H]⁺ calcd. for C₁₉H₁₅NO₄: 322.1079, found 322.10835.

2.1.2.4. (E)-4-(((4-oxo-4H-chromen-3-yl)methylene)amino)benzoic acid (4)

NaOH (0.056 g, 1.4 mmol) was added to a solution of (E)-ethyl 4-(((4-oxo-4H-chromen-3-yl)methylene)amino)benzoate **3** (0.15 g, 0.47 mmol) in methanol, THF, and water (2:1:2). The mixture was stirred at RT for 18 hrs. After the complete disappearance of the ester, the solvent was evaporated under vacuum, and the residue was triturated with HCl (5M) till PH = 5. The resulting solid was collected by filtration and purified by flash column chromatography eluting with DCM/ methanol (9:1) then further purified using preparative TLC using DCM/ methanol (9.5:0.5) as an eluting system to produce the designated compound **4** as yellow solid (0.025 g, 17.9%) m.p. 291-292°C. ¹H NMR (400 MHz, DMSO): δ 11.84 (s, 1H, OH), 8.18 (d, J = 12.4 Hz, 1H, CH=N), 7.95 (d, J = 8.0 Hz, 2H, ArH), 7.85 (d, J = 7.6 Hz, 1H, ArH), 7.55 (t, J = 7.8 Hz, 1H, ArH), 7.47 (d, J = 8.2 Hz, 2H, ArH), 7.12 (dt, J = 20.5, 7.8 Hz, 2H, ArH), 5.97 (s, 1H, ArH). ¹³C NMR (101 MHz, DMSO): δ 173.27, 167.24, 156.12, 144.53, 131.62, 125.94, 125.64, 122.44, 118.58, 118.41, 116.61, 113.06, 105.36,

100.39, 93.59. **FT-IR** (ν max, cm^{-1}): 3356 (broad, OH), 2968 (C-H aromatic), 1650 (C=O acid), 1587 (C=N), 1558 (C=C). **HRMS** (ESI) m/z $[\text{M} + \text{H}]^+$ calcd. for $\text{C}_{17}\text{H}_{11}\text{NO}_4$: 294.0766, found 294.07707.

2.1.2.5. (E)-ethyl3-(4-oxo-4H-chromen-3-yl)acrylate (5)

Yield 96% as yellow solid, m.p. 96-98°C (as reported) [28]. **^1H NMR (400 MHz, DMSO)** δ 8.90 (s, 1H, ArH), 8.13 (d, $J = 8.0$ Hz, 1H, ArH), 7.84 (t, $J = 7.6$ Hz, 1H, ArH), 7.70 (d, $J = 8.4$ Hz, 1H, ArH), 7.60 – 7.40 (m, 2H, CH=CH, ArH), 7.18 (d, $J = 16.0$ Hz, 1H, CH=CH), 4.18 (q, $J = 7.8$ Hz, 2H, OCH₂CH₃), 1.26 (t, $J = 7.4$ Hz, 3H, OCH₂CH₃).

2.1.2.6. (E)-N-hydroxy-3-(4-oxo-4H-chromen-3-yl)acrylamide (6)

To a solution of ester **5** (10 g, 0.0409 mol) dissolved in 10 ml ethanol, a freshly prepared hydroxylamine solution, prepared by dissolving hydroxylamine hydrochloride (85.26 g, 1.227 mol) in Na ethoxide solution (9.407 g, 0.409 mol Na metal in 50 ml ethanol), was added portion wise. The mixture was heated under reflux at 80°C for 6 hrs. The reaction was cooled and evaporated under *a vacuum*. The residue was triturated with 100 ml iced HCl solution (10%) portionwise and then extracted with (50 ml *3) diethyl ether. The organic layer was dried over anhydrous MgSO_4 and evaporated under *vacuum* to afford a residue that was purified by using preflash column chromatography eluting with DCM and methanol (9.4:0.6) yielding the titled compound **6** as buff solid (0.05 g, 0.5%); m.p.295-297°C. **^1H NMR (400 MHz, DMSO)**: δ 11.73 (s, 1H, OH), 10.36 (s, 1H, NH), 8.21 (s, 1H, ArH), 7.40 – 7.20 (m, 2H, ArH), 7.13 (d, 1H, ArH), 6.99 – 6.80 (m, 2H, CH=CH and ArH), 6.54 (d, 1H, CH=CH). **^{13}C NMR (101 MHz, DMSO)**: δ 175.20, 161.41, 157.07, 153.07, 137.14, 130.67, 130.58, 119.26, 116.79,

112.28. **FT-IR** (ν max, cm^{-1}): 3500 (OH/NH broad), 2923 (C-H aromatic), 1626 (C=O hydroxamic acid), 1526 (C=C). **HRMS** (ESI) m/z $[\text{M} + \text{H}]^+$ calcd. for $\text{C}_{12}\text{H}_9\text{NO}_4$: 232.0610, found 230.2478.

2.2. Molecular Modeling

The molecular docking was performed using Autodock Vina. The protein and ligand were prepared before docking through Accelrys Discovery Studio. The dimensions of the binding site, which is known as the grid box, were determined by using Autodock tools. The analysis and visualization of the results were conducted using multiple software like PyMol, Autodock tools, and Discovery Studio.

2.2.1. Protein Preparation

The X-ray crystallography structures of homosapien HDAC6 cocrystallized with TSA and HDAC8 cocrystallized with TSA (PDB codes: 5edu and 1t64, respectively) were obtained from the Protein Data Bank (PDB) by using the website of Research Collaboration for Structural Bioinformatics (RCSB). Each structure was loaded in Accelrys Discover Studio where the preparation of protein took place. This was done by utilizing the protein preparation tools embedded in the software. The steps included adding hydrogens, completing missing residues, applying CHARMM forcefield, and energy minimization via the Adopted Basis NR algorithm. To ensure that the main conformation and configuration of the protein wouldn't be affected by the changes taken during the minimization step, a constraint was created to surround any atom other than the added hydrogens by the software. After that, the prepared protein with its cocrystallized ligand was viewed using Autodock tools where the dimensions of the grid box were determined based on our knowledge of the essential amino acids in the binding site. Finally, the ligand was

cleared, and subsequently, the target was ready for the docking process.

2.2.2. Ligand Preparation

Ligands were sketched in the Discovery Studio to be available in the 3D structures. They were prepared via ligand preparation protocol that is integrated into Drug Discovery software. The preparation involved adding polar hydrogens, typing with CHARMM force field, energy minimization via SMART minimizer algorithm, confirmation generation, and passing through the Lipinski filter. Also, the ligand preparation protocol enabled the ionization of the sketched ligands according to pH which is usually adjusted to 7.4 to simulate the physiological conditions. In the current study, no isomers or tautomers were generated.

2.2.3. Docking Process

The docking step was carried out using Autodock Vina Software, which first reconsidered the charge distribution in the protein to guarantee that the zinc atom is carrying a 2+ charge since HDAC is a metalloprotein in which Zinc binding is the most crucial interaction for the activity. Then the software utilized the given dimension of the grid box to generate a built-in autogrid for the binding site in which the types and energy of each atom were taken into consideration. Finally, the software searched for different poses for each ligand in the generated grid to produce poses close to the bioactive conformer. Usually, it generates nine conformers that are ranked according to the energy of their binding affinity to the target. The energy is calculated based on the force field rules. The more negative the energy of binding affinity was, the more stable the complex we got [29]. The results were displayed as a PDBQT file containing the poses generated without the target and they can be separated by using a tool called Vina Split. The protein and pose file can be

reopened in different software to analyze the best pose of the ligand in the binding site and display the interactions between the ligand and amino acid residues in the active site. One of the programs used was PyMol which is distinguished by its ability to perfectly display the polar interactions involving metal chelation and hydrogen bonds that were essential for activity in our case. Also, Discovery Studio was used for producing 2D and 3D interaction diagrams.

2.3. HDAC Isoforms Assay

The *in vitro* HDAC inhibition assay for the synthesized compound against HDAC 1,6, and 8 isoforms was performed in BPS Bioscience Corporation. The enzyme activity assay utilized HDAC 1 (BPS #50051), HDAC 6 (BPS #50006), and HDAC 8 (BPS #50008) as the enzyme sources. The assay was done based on the established experimental procedure by Bioscience (Supplementary).

2.4. Antiproliferative Activity against Cancer Cell Lines

The NCI *in vitro* anticancer screening begins with the evaluation of the tested compounds at a single dose of 10 mM against the full NCI 60 cell lines panel. These cancer cell lines involve leukemia, non-small cell lung (NSCLC), melanoma, colon, CNS, ovarian, renal, and prostate. and breast cancer. The screening procedure is carried out according to the standard experimental conditions as reported on the official website of the NCI [30].

3. Results and Discussion

3.1. Rational and Design

According to our knowledge of the essential structural characteristics that are crucial for the inhibitory activity of HDACs. We tried to design novel compounds with potential activity against HDACs. For the SRM, we selected a benzopyranone scaffold that resembles the

naturally occurring chromones and coumarins that are famous for their variable biological effects such as anti-inflammatory, anti-cancer, antimicrobial, and anti-allergic [31]. It is revealed that the anticancer effect of chromones is achieved through several pathways including blocking cell cycles and consequently inhibiting proliferation, inducing apoptosis, angiogenesis suppression, trapping cancer cells, and hence limiting the metastasis and immunomodulation. However, the detailed underlying mechanism of action isn't fully understood yet [32]. That's why chromone was selected as the SRM in our design to synergize the normal HDACi effect and maximize the potency of the designated compounds besides lowering the toxic effects on normal cells. Concerning the linker, the vinyl linker was chosen as a trial to mimic TSA, Belinostat, and Panobinostat. The vinyl increases lipophilicity which is necessary to outweigh the hydrophilicity of the zinc chelating moiety so enhances the pharmacokinetic properties like absorption and cell permeability [33]. In addition, the vinylic linker limits the rotation around a single bond and subsequently rigidifies the compound in certain confirmation that keeps the required distances and configurations between the binding groups and the corresponding amino acids in the binding site enhancing the binding affinity between ligand and target which in turn

reflected on the activity and potency [34]. Finally, hydroxamic acid was preferred due to its powerful zinc binding affinity as illustrated in Fig. 3.

The designed compound was first evaluated for its predicted activity against HDAC 6 and 8 in comparison to TSA by molecular docking using Autodock Vina software. We used HDAC6 and HDAC8 isoenzymes co-crystallized with Trichostatin A (PDB codes: 5edu and 1t64, respectively).

Upon analysis of the binding of the cocrystallized TSA and compound 6 in HDAC6 isoform binding site. TSA showed essential interactions involving the pi sigma interactions with PHE 620, PHE 680, and hydrogen bonding with HIS 610, HIS 611, and ASP 649 as illustrated in Fig. 4. A.

Regarding compound 6, it achieved a binding affinity energy of -7.368 Kcal/mol, which is comparable to that of TSA, binding affinity energy = -8.369. Also, it displayed the essential key interactions performed by TSA. These interactions include the pi interaction with PHE 620 and the hydrogen bonds with HIS 610, HIS 611, and ASP 649 as shown in Fig. 4. B, besides the zinc-binding which is confirmed through visualizing the complex using PyMol as shown in Fig. 4. C.

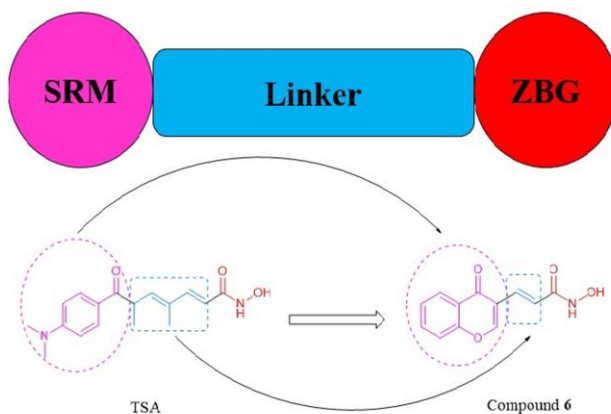


Fig. 3. The strategy of designing compound 6 based on TSA pharmacophore

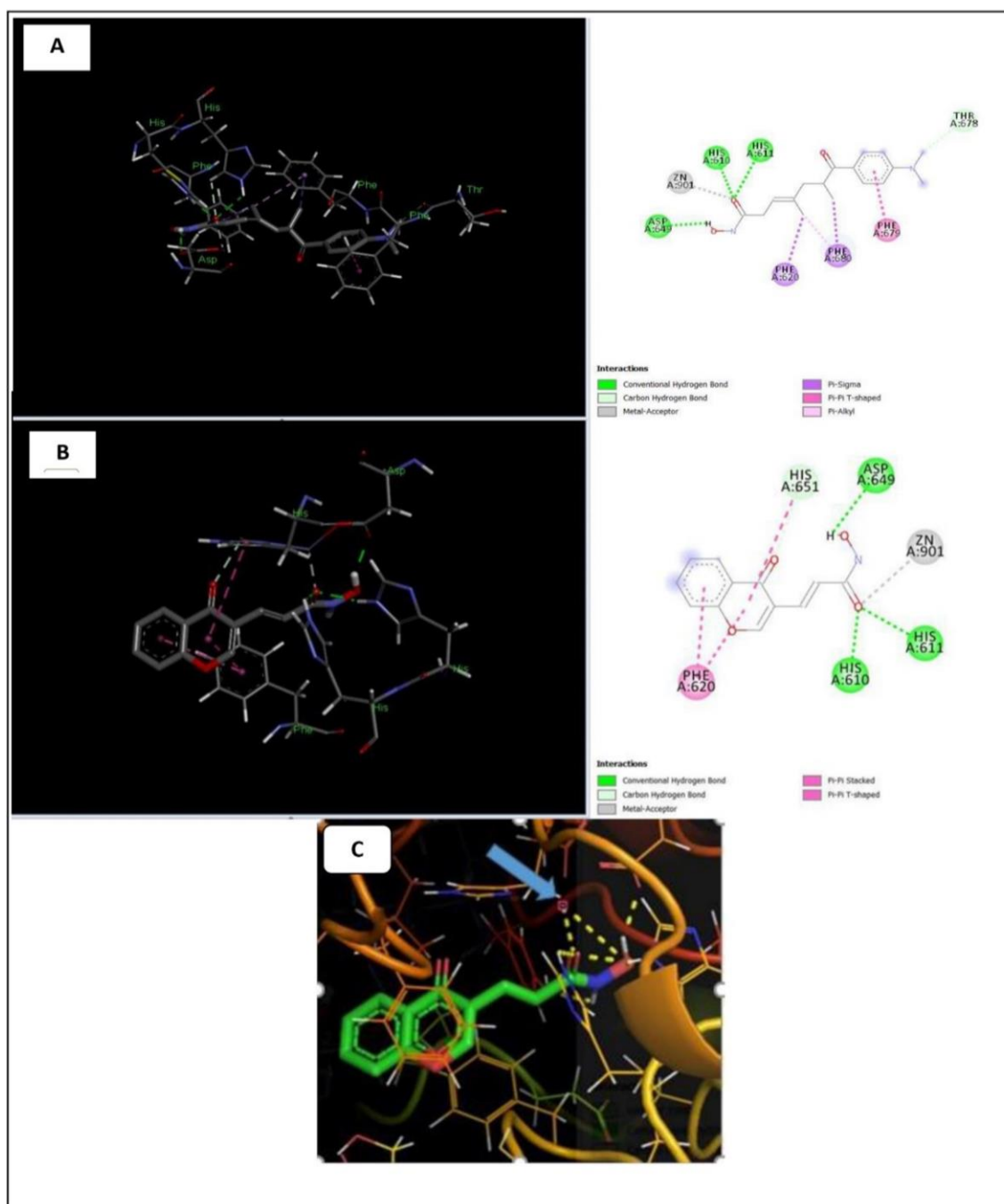


Fig. 4. (A) 2D and 3D binding diagrams of cocrystallized TSA in HDAC6. (B) 2D and 3D binding interactions of compound 6 in HDAC6 active site. Gray dashed lines: metal acceptor, Green dashed lines: hydrogen bonding, Purple dashed lines: pi sigma interactions, Pink dashed lines: pi-pi interaction. (C) 3D interaction diagram showing the metal chelation between the two oxygen atoms of hydroxamic acid moiety in compound 6 and the Zn atom in HDAC6, where the arrow is pointing to the Zn atom.

Also, we investigated the binding between cocrystallized TSA and HDAC 8 to detect the amino acid residues involved in the crucial interactions for the activity. These interactions

involved pi interactions with PHE 152 and PHE 208 and hydrogen bonding with HIS 142, HIS 143, ASP 178, and TYR 306 as described in **Fig. 5. A.**

Upon analyzing the result of docking of compound 6 in HDAC 8 isoform, it was found that it displayed binding affinity energy = -7.454 Kcal/mol which is close to that of TSA with binding affinity = -8.1 kcal/mol. Additionally, it preserved the vital interactions as shown in the cocrystallized ligand. These interactions include

Pi interactions with PHE 152 and HIS 180 and hydrogen bonding with HIS 142, HIS 143, and ASP 178 as illustrated in **Fig. 5. B**. The zinc-binding was obvious through the interaction with the two oxygen atoms in the hydroxamic acid chelating group as shown in **Fig. 5. C**.

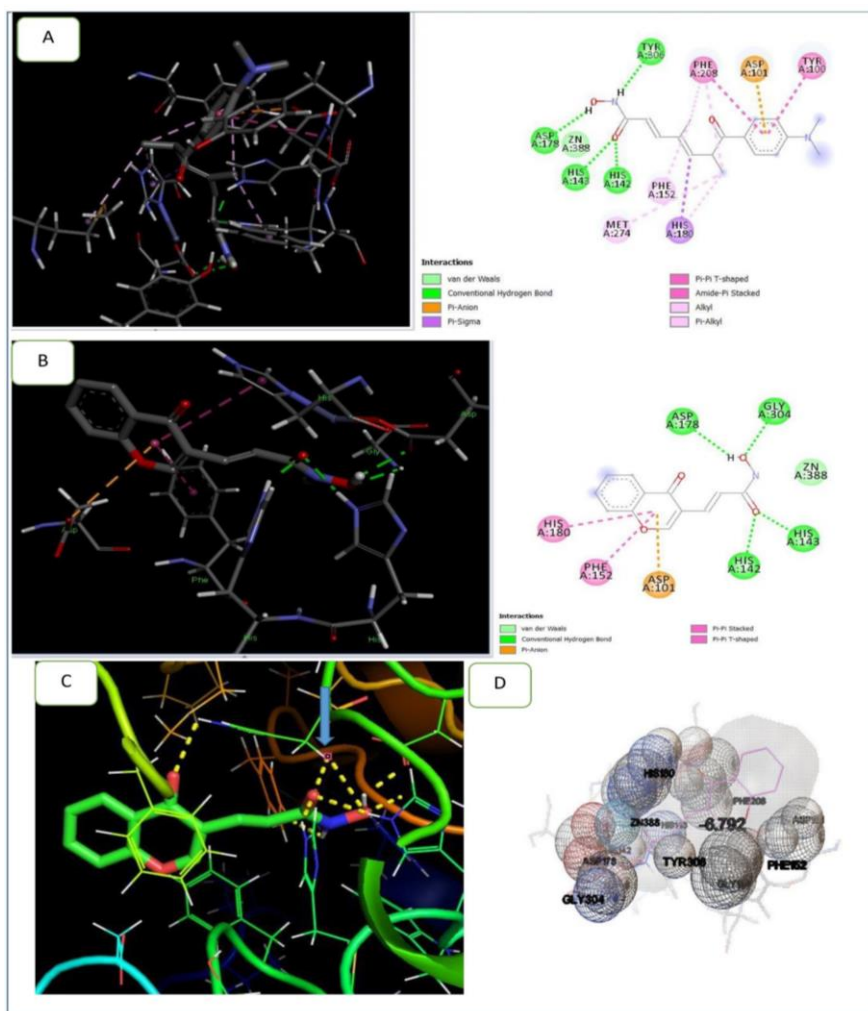


Fig. 5. (A) 2D and 3D representations of the interactions between TSA and amino acids in HDAC8 active site. (B) 2D and 3D interaction diagrams displaying the binding between compound 6 and amino acid residues in HDAC8 active site. Green dashed lines: hydrogen bonding, Purple dashed lines: pi sigma interactions, Pink dashed lines: pi-pi interaction, Orange dashed lines: pi-anion interaction. (C) 3D interaction diagram showing the metal chelation between the two oxygen atoms of hydroxamic acid moiety in compound 6 and the Zn atom in HDAC8, where the arrow is pointing to the Zn atom. (D) Autodock representation of the interactions between compound 6 and HDAC 8 showing zinc metal atom and all amino acid residues that come into contact with the tested compound.

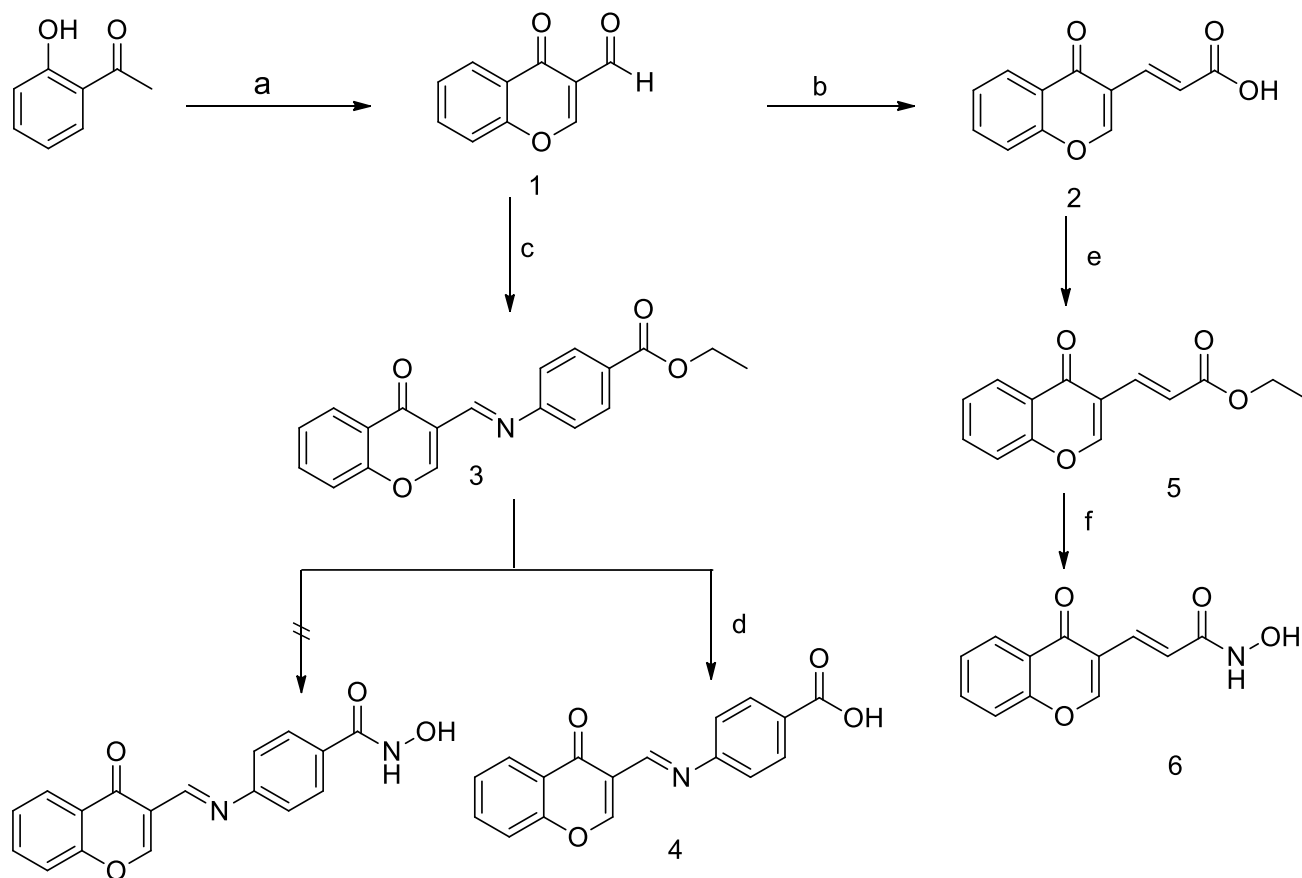
3.2. Chemistry

For the synthesis of *(E)-N-hydroxy-3-(4-oxo-4H-chromen-3-yl)acrylamide* **6**, 2-

hydroxyacetophenone was cyclized into 3-formyl chromone **1** by the traditional Vilsmeier Haack reaction [35]. Then the resulting carbaldehyde **1**

was condensed with 4-aminobenzoate ester through a nucleophilic addition reaction to produce the corresponding Schiff's base **3** in which glacial acetic acid was selected as a catalyst to absorb the resulting water [36, 37]. It was proposed to synthesize the hydroxamic acid derivative by reacting the activated ester with hydroxylamine, which is a strong nucleophile. However, it failed, maybe due to the pH sensitivity of the imine, as we found that the imine-based compounds are stable in a very narrow range of pH from 4.8 to 7 and this range isn't applicable to be achieved during the synthesis of hydroxamic acids [38]. So, we decided to prepare the corresponding carboxylic

acid derivative **4** instead via the alkaline ester hydrolysis reaction [39] of Schiff's base **3** with careful monitoring of pH throughout the reaction and workup. The produced carbaldehyde **1** was also reacted with malonic acid through the Knoevenagel condensation reaction [40] yielding the acrylic acid derivative **2** which was then esterified using the simple Fischer reaction [41] to obtain the ester derivative **5**. Synthesis of the ester was essential to activate the nucleophilic substitution reaction with the hydroxylamine hydrochloride to give the hydroxamic acid [42] derivative **6** in the presence of a strong base like sodium ethoxide or methoxide [43]. **Scheme 1**



Scheme 1. Reagents and Conditions (a) POCl_3 , DMF, reflux 4 h, RT, 20 hrs. (b) malonic acid, pyridine, reflux 2 hrs. (c) ethyl 4-aminobenzoate, ethanol, glacial acetic acid, reflux 12 hrs. (d) NaOH, methanol, water, THF, RT, 18 hrs. (e) ethanol, conc. H_2SO_4 , reflux 12 hrs. (f) $\text{NH}_2\text{OH}\cdot\text{HCl}$, Na ethoxide, ethanol, reflux 4-6 hrs.

3.3. Biological Evaluation

3.3.1. *In Vitro* HDAC Inhibition Assay

The synthesized compound **6** was assessed for its inhibitory activity against HDAC1, 6, and 8 isoforms at two concentrations, 1 and 10 μM , by BPS Bioscience Company in the USA. On HDAC 1 isoenzyme, it showed 3% inhibition at 1 μM concentration. However, the inhibitory activity increased to 14% upon increasing the concentration to 10 μM . On HDAC 6 isoform,

the result was very disappointing since it achieved only 4% inhibition at 1 μM and diminished activity at 10 μM concentration. On HDAC 8 isoform, it showed 14% inhibition at a concentration of 10 μM but the inhibitory activity diminished completely at 1 μM concentration. The results are displayed in **Table 1** with a comparison to the positive control **SAHA** that was selected for HDAC 1 and 6 isoforms and **TSA** for HDAC 8.

Table 1. Effect of compound 6 against different HDAC isoforms

concentration	% Inhibition		
	HDAC1	HDAC6	HDAC8
1 μM	3	4	0
10 μM	14	0	14
SAHA, 0.01 μM	35	15	-
SAHA, 0.1 μM	64	67	-
SAHA, 1 μM	90	95	-
TSA, 0.1 μM	-	-	2
TSA, 1 μM	-	-	33
TSA, 10 μM	-	-	87

3.3.2. Antiproliferative Activity

Compound **6** was selected by the National Cancer Institute (NCI) in the USA through the Development Therapeutics Programme (DTP) for evaluating antineoplastic activity. Its NCI code is D-845172/1. It was screened against different types of human cancer cell lines. The screening was performed on the 60-cell panel of NCI using a single dose concentration of 10 μM . The result was reported in tabular and graph forms as

described in **Fig. 6**. The result represents the growth percent of the cells treated with the tested compound in comparison to the untreated control cells. Compound **6** induces 24.5% inhibition on the UO-31 cell line of renal cancer and 14.5 % on the BT-549 cell line of breast cancer. The result was very reliable and compatible with the enzyme assay as many recent studies confirm the overexpression of class I HDACs in renal [44] and some types of breast cancers particularly HDAC1 [45].

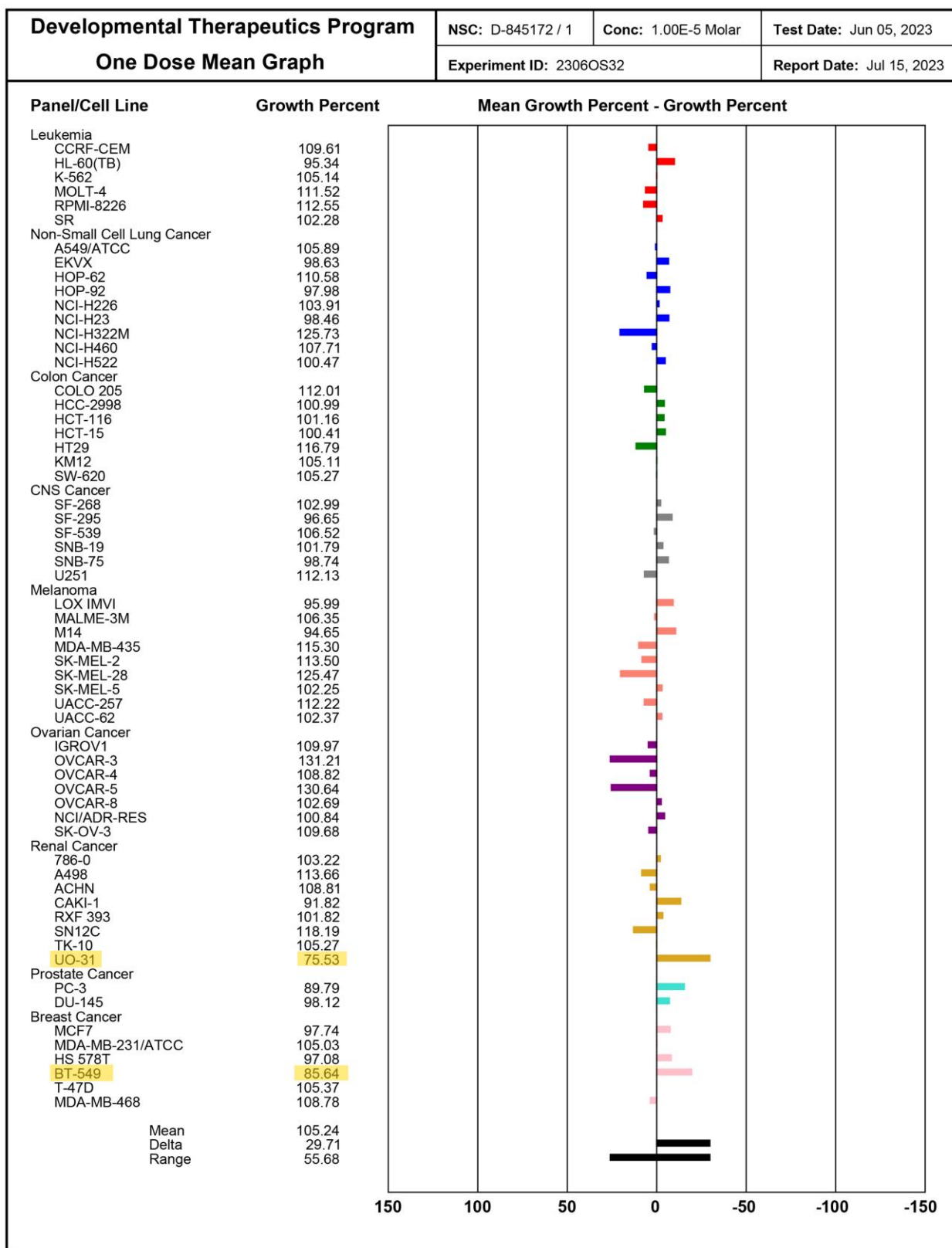


Fig. 6. The effect of compound 6 on the NCI 60-cell panel

Conclusion

Herein, we designed and synthesized a novel chromene-based HDAC inhibitor depending on the common pharmacophore and the prospective data of the molecular modeling studies. In the designed compound, the benzopyranone ring acted as SRM, the vinyl moiety acted as a linker, and hydroxamic acid behaved as a metal chelator. The inhibitor displayed 25% inhibition on the UO-31 that is one of the NCI renal cancer cell lines and has 15% inhibition on the breast cancer cell line BT-549. It also showed 14% inhibitory activity on HDAC 1 and 8 isoforms. It is demonstrated that the designed compound has the potential to be a selective class I HDAC inhibitor but it needs further structural optimizations for enhancing its activity and selectivity. We recommend increasing the length of the linker so that the ZBG is closer to the metal, attaining stronger chelation and higher binding affinity which subsequently, will be reflected in the inhibitory activity against the enzyme and on the growth of cancer cells.

Declarations

Consent to publish

All authors have read and agreed to the published version of the manuscript

Ethics approval and consent to participate

Not applicable

Availability of data and material

All data generated or analyzed during this study are included in this published article in the main manuscript.

Competing interests

The authors have no financial or non-financial benefits to relate.

Funding

The authors declare that no grants, funds, or any other support were gained during manuscript preparation.

Author contribution

Rosaline Ashraf reviewed the literature and prepared the manuscript. Mai Adel revised the manuscript. K. A. Abouzid and Rabah A. T. Serya supervised the preparation of the manuscript. All the authors reviewed the manuscript.

Acknowledgments

I owe my deepest appreciation to the National Cancer Institute, USA for performing the in vitro 60-cell lines anticancer assay. I am grateful to BPS Bioscience for the HDAC inhibition assay. I would like to thank the Center for Drug Discovery Research and Development, Ain Shams University, for performing the NMR and IR spectroscopy. Also, I would like to thank Dr. Khalid Agha in the Natural Products Research Center, Fayoum University for performing HRMS.

4. References

1. Ruijtenberg S, van den Heuvel S. Coordinating cell proliferation and differentiation: Antagonism between cell cycle regulators and cell type-specific gene expression. *Cell cycle*. 2016 Jan 17;15(2):196-212.
2. Khan O, La Thangue NB. HDAC inhibitors in cancer biology: emerging mechanisms and clinical applications. *Immunol Cell Biol*. 2012 Jan;90(1):85-94.
3. Xia JK, Qin XQ, Zhang L, Liu SJ, Shi XL, Ren HZ. Roles and regulation of histone acetylation in hepatocellular carcinoma. *Front Genet*. 2022 Aug 25;13:982222
4. Kriswiastiny R, Partan RU, Darma S, Reagan M. The Role of Histone Deacetylase and Histone Deacetylase Inhibitors in Rheumatoid Arthritis. *Biosci Med J*

- Biomed Transl Res. 2021 Nov 5;5(11):1103-10.
5. Harrington KJ, Nenclares P. The biology of cancer. *Medicine (Baltimore)*. 2022.
 6. Kashyap D, Garg VK, Sandberg EN, Goel N, Bishayee A. Oncogenic and Tumor Suppressive Components of the Cell Cycle in Breast Cancer Progression and Prognosis. *Pharmaceutics* 2021, 13, 569.
 7. Oing C, Skowron MA, Bokemeyer C, Nettersheim D. Epigenetic treatment combinations to effectively target cisplatin-resistant germ cell tumors: past, present, and future considerations. *Andrology*. 2019 Jul;7(4):487-97.
 8. Lee JE, Kim MY. Cancer epigenetics: Past, present and future. In *Semin Cancer Biol*. 2022 Aug 1 (Vol. 83, pp. 4-14).
 9. Vaidya GN, Rana P, Venkatesh A, Chatterjee DR, Contractor D, Satpute DP, et al. Paradigm shift of “classical” HDAC inhibitors to “hybrid” HDAC inhibitors in therapeutic interventions. *Eur J Med Chem*. 2021 Jan 1;209:112844.
 10. Ganesan A. Epigenetic drug discovery: a success story for cofactor interference. *Philos Trans R Soc B Biol Sci*. 2018 Jun 5;373(1748):20170069.
 11. Waltregny D, De Leval L, Glénisson W, Tran SL, North BJ, Bellahcène A, Weidle U, Verdin E, Castronovo V. Expression of histone deacetylase 8, a class I histone deacetylase, is restricted to cells showing smooth muscle differentiation in normal human tissues. *Am J Pathol*. 2004 Aug 1;165(2):553-64.
 12. Thiagalingam SA, CHENG KH, Lee HJ, Mineva N, Thiagalingam A, Ponte JF. Histone deacetylases: unique players in shaping the epigenetic histone code. *Ann N Y Acad Sci*. 2003 Mar;983(1):84-100.
 13. Ruijter AJ, GENNIP AH, Caron HN, Kemp S, KUILENBURG AB. Histone deacetylases (HDACs): characterization of the classical HDAC family. *Biochem J*. 2003 Mar 15;370(3):737-49.
 14. Vannini A, Volpari C, Gallinari P, Jones P, Mattu M, Carfi A, et al. Substrate binding to histone deacetylases as shown by the crystal structure of the HDAC8–substrate complex. *EMBO Rep*. 2007 Sep;8(9):879-84.
 15. Zhang L, Zhao W, Chen H, Cui Y. Enzymatic synthesis of phenol polymer and its functionalization. *J Mol Catal B Enzym*. 2013 Mar 1;87:30-6. <https://doi.org/10.1016/j.molcatb.2012.10.015>.
 16. Karagiannis D, Rampias T. HDAC inhibitors: dissecting mechanisms of action to counter tumor heterogeneity. *Cancers*. 2021 Jul 16;13(14):3575.
 17. Kumar B, Yadav A, Lang JC, Teknos TN, Kumar P. Suberoylanilide hydroxamic acid (SAHA) reverses chemoresistance in head and neck cancer cells by targeting cancer stem cells via the downregulation of Nanog. *Genes Cancer*. 2015 Mar;6(3-4):169.
 18. Qiu X, Zhu L, Wang H, Tan Y, Yang Z, Yang L, Wan L. From natural products to HDAC inhibitors: An overview of drug discovery and design strategy. *Bioorg Med Chem*. 2021 Dec 15; 52:116510.
 19. De Souza C, Chatterji PB. HDAC inhibitors as novel anti-cancer therapeutics. *Recent Pat Anticancer Drug Discov*. 2015 May 1;10(2):145-62.

20. Yoon S, Eom GH. HDAC and HDAC inhibitor: from cancer to cardiovascular diseases. *Chonnam Med J.* 2016 Jan;52(1):1-1.
21. Gao S, Li X, Zang J, Xu W, Zhang Y. Preclinical and clinical studies of chidamide (CS055/HBI-8000), an orally available subtype-selective HDAC inhibitor for cancer therapy. *Anti-Cancer Agents Med Chem (Formerly Curr Med Chem Anti-Cancer Agents).* 2017 May 1;17(6):802-12.
22. Wang F, Lu W, Zhang T, Dong J, Gao H, Li P, et al. Development of novel ferulic acid derivatives as potent histone deacetylase inhibitors. *Bioorg Med Chem.* 2013 Nov 15;21(22):6973-80.
23. Miller TA, Witter DJ, Belvedere S. Histone deacetylase inhibitors. *J Med Chem.* 2003 Nov 20;46(24):5097-116.
24. Suzuki T, Miyata N. Non-hydroxamate histone deacetylase inhibitors. *Curr Med Chem.* 2005 Nov 1;12(24):2867-80.
25. Zhao P, Li J, Yang G. Synthesis and insecticidal activity of chromanone and chromone analogues of diacylhydrazines. *Bioorg Med Chem.* 2007;15, 1888–1895. <https://doi.org/10.1016/j.bmc.2007.01.008>.
26. Nohara A, Umetani T, Sanno Y. Studies on antianaphylactic agents—I. *Tetrahedron.* 1974;30(19):3553-61.
27. Chand K, Tiwari RK, Kumar S, Shirazi AN, Sharma S, Van der Eycken EV, et al. Synthesis, Antiproliferative, and c-Src Kinase Inhibitory Activities of 4-Oxo-4H-1-benzopyran Derivatives. *J Heterocycl Chem.* 2015 Mar;52(2):562-72. <https://doi.org/10.1002/jhet>.
28. Kumar S, Singh BK, Pandey AK, Kumar A, Sharma SK, Raj HG, et al. A chromone analog inhibits TNF- α induced expression of cell adhesion molecules on human endothelial cells via blocking NF- κ B activation. *Bioorg Med Chem.* 2007 Apr 15;15(8):2952-62. <https://doi.org/10.1016/j.bmc.2007.02.004>
29. Trott O, Olson AJ. AutoDock Vina: improving the speed and accuracy of docking with a new scoring function, efficient optimization, and multithreading. *J Comput Chem.* 2010 Jan 30;31(2):455-61.
30. NCI-60 Screening Methodology | NCI-60 Human Tumor Cell Lines Screen | Discovery & Development Services | Developmental Therapeutics Program (DTP), (n.d.).
31. Sosnovskikh VY. Synthesis and Reactivity of Electron-Deficient 3-Vinylchromones. *SynOpen.* 2021 Jul;5(03):255-77. <https://doi.org/10.1055/a-1589-9556>.
32. Islam R, Hossain MS, Mock PY, Leong SW, Lam KW. Exploring the potential of chromone scaffold compounds in cancer therapy: targeting key kinase pathways. *Med Chem Res.* 2023 Apr 20:1-22.
33. Waring MJ. Lipophilicity in drug discovery. *Expert Opin Drug Discov.* 2010 Mar 1;5(3):235-48.
34. Wiene-Schmidt B, Jonker HR, Wulsdorf T, Gerber HD, Saxena K, Kudlinzki D, et al. Paradoxically, the most flexible ligand binds most entropy-favored: intriguing impact of ligand flexibility and solvation on drug-kinase binding. *J Med Chem.* 2018 Jun 16;61(14):5922-33.

35. Ali TE, Ibrahim MA, El-Gohary NM, El-Kazak AM. 3-Formylchromones as diverse building blocks in heterocycles synthesis. *Eur J Chem.* 2013 Sep 30;4(3):311-28.
<https://doi.org/10.5155/eurjchem.4.3.311>.
36. Innasiraj A, Anandhi B, Gnanadeepam Y, Das N, Paularokiadoss F, Ilavarasi AV, et al. Experimental and theoretical studies of novel Schiff base based on diammino benzophenone with formyl chromone–BPAMC. *J Mol Struct.* 2022 Oct 5;1265:133450.
<https://doi.org/10.1016/j.molstruc.2022.133450>.
37. Rathelot P, Azas N, El-Kashef H, Delmas F, Di Giorgio C, Timon-David P, et al. 1, 3-Diphenylpyrazoles: synthesis and antiparasitic activities of azomethine derivatives. *Eur J Med Chem.* 2002 Aug 1;37(8):671-9.
[https://doi.org/10.1016/S0223-5234\(02\)01388-0](https://doi.org/10.1016/S0223-5234(02)01388-0).
38. Hine J, Craig Jr JC, Underwood JG, Via FA. Kinetics and mechanism of the hydrolysis of N-isobutylidenemethylamine in aqueous solution. *J Am Chem Soc.* 1970 Aug;92(17):5194-9.
<https://doi.org/10.1021/ja00720a032>.
39. Parekh VJ, Rathod VK, Pandit AB. Substrate hydrolysis: Methods, mechanism, and industrial applications of substrate hydrolysis. Academic Press. 2011. doi <https://doi.org/10.1016/B978-0-08-088504-9.00094-5>.
40. van Schijndel J, Canalle LA, Molendijk D, Meuldijk J. The green Knoevenagel condensation: solvent-free condensation of benzaldehydes. *Green Chem Lett Rev.* 2017 Oct 2;10(4):404-11.
<https://doi.org/10.1080/17518253.2017.1391881>.
41. Khan Z, Javed F, Shamair Z, Hafeez A, Fazal T, Aslam A, et al. Current developments in esterification reaction: A review on process and parameters. *J Ind Eng Chem.* 2021 Nov 25;103:80-101.
<https://doi.org/10.1016/j.jiec.2021.07.018>.
42. Sandler SR, Karo W. Organic functional group preparations. 2013.
43. Reddy AS, Kumar MS, Reddy GR. A convenient method for the preparation of hydroxamic acids. *Tetrahedron Letters.* 2000 Aug 12;41(33):6285-8.
[https://doi.org/10.1016/S0040-4039\(00\)01058-3](https://doi.org/10.1016/S0040-4039(00)01058-3).
44. Fritzsche FR, Weichert W, Röske A, Gekeler V, Beckers T, Stephan C, et al. Class I histone deacetylases 1, 2, and 3 are highly expressed in renal cell cancer. *BMC Cancer.* 2008 Dec;8(1):1-0.
45. Müller BM, Jana L, Kasajima A, Lehmann A, Prinzler J, Budczies J, et al. Differential expression of histone deacetylases HDAC1, 2, and 3 in human breast cancer—overexpression of HDAC2 and HDAC3 is associated with clinicopathological indicators of disease progression. *BMC Cancer.* 2013 Dec;13(1):1-8.
<https://doi.org/10.1186/1471-2407-13-215>.